4. TOMOGRAPHIC GAMMA-RAY SCANNING OF URANIUM AND PLUTONIUM

J. Steven Hansen

INTRODUCTION

Development of the Tomographic Gamma-ray Scanning (TGS) technology began in the early 1990's (Refs. 1-3) in response to an increasing demand to assay a class of materials that were difficult or impossible to assay quickly and accurately with existing NDA techniques. The problem materials exhibited arbitrary distributions of nuclear material in a matrix of extreme heterogeneity in both density and composition. Techniques which volume averaged over these heterogeneities often led to large errors and, given the difficulty of preparing representative standards, error estimates for any arbitrary samples were not reliable.

What was needed was a technique capable of viewing the sample as a composite of small volumes combined with a means of estimating the mass of the target isotopes within each small volume. Combining the principles of tomography with the power of high resolution gamma-ray spectroscopy, the TGS technique was conceptualized and within a decade the TGS technique developed into one of the most robust, versatile NDA methods used in safeguards and nuclear waste measurements across the DOE complex.

The next section describes the underlying principles of TGS at a fundamental level leaving a more detailed discussion to the TGS application guide (Ref. 4). Nevertheless, we do present here a set of idealized image reconstruction problems to provide the reader with a good conceptual feel for the general mathematical approach underlying tomographic image reconstruction. A description of the hardware modules making up a typical TGS instrument then is provided. Where appropriate we try to provide helpful design criteria and guidance for systems to be used in production applications. To assist the reader in assessing the applicability of TGS to a particular class of materials, a section on its performance then follows. The Performance Demonstration Program (PDP), sponsored by the Waste Isolation Pilot Plant (WIPP) in Carlsbad, NM, is a series of blind tests with standard waste drums designed to simulate typical materials destined to be shipped to WIPP for burial. All of the accepted NDA techniques for measurements of such materials were represented in the tests and the results provide an excellent starting point for the reader responsible for selecting the correct instruments for a particular task. Two real-life examples are given that illustrate the cost-benefit of TGS for certain classes of materials for which other NDA techniques are not well suited. The first example involves plutonium laden electro-refining salt residues at the Rocky Flats Environmental Technology Site (RFETS) in Golden, CO, and the second describes its application to a large inventory of 208-ℓ (55-gal.) drums containing uranium contaminated materials. These examples illustrate that the high throughput and low bias of the TGS technique demonstrated in the PDP can carry over to the production environment when appropriate controls are applied and systems are properly designed. The principal limitation of the TGS for the assay of uranium and plutonium arises from the propensity for high-Z materials to strongly attenuate their own gamma-rays. The extreme example of this problem is the self-attenuation of gamma rays in lumps of uranium (Z=92) and plutonium (Z=94). In materials that may contain these elements in non-microscopic sizes, a method for recognizing these conditions must exist and appropriate corrections must be applied to eliminate biases. A section is devoted to the subject of lump corrections, because of importance for the broader class of materials that are found in nuclear facilities. The TGS

technology is now quite mature and available commercially and the final section describes some designs available from commercial vendors.

MEASUREMENTS PRINCIPLES

A. General Concepts

In 1895, at the young age of 50, William Conrad Roentgen (1845-1923), working with a cathode ray tube (CRT), discovered quite by accident that some fluorescent crystals across the room gave off a green glow when the machine was on, even when the CRT was shrouded with a black cloth impenetrable by light. Such was the discovery of ionizing radiation that Roentgen named x rays. Roentgen quickly followed his discovery by becoming the world's first radiologist, exposing films with various objects, including his wife's hand (Figure 1), placed between the CRT and the film. Within a year, battle surgeons were using x rays to locate bullets in wounded soldiers and Henri Becquerel had discovered natural radioactivity. The atomic age was born.

Radiographs such as that of Mrs. Roentgen's hand have been critical tools in the fields of medical and industrial diagnostics. The radiographic technique consists of focusing a broad parallel beam of penetrating radiation upon a sample of interest and recording the effects of the unabsorbed portion of the beam upon the radiographic film. The picture or image provided by the film is really just a representation of the opacity of the sample, which varies dependant

Fig. 1 *Radiograph of Mrs. Roentgen's hand.*

upon its density, thickness, and atomic number (Z). In the case of a biological sample such as Mrs. Roentgen's hand, the calcium in the bones is of higher atomic number (Z=22) and density

than the surrounding flesh and preferentially attenuates the beam and correspondingly underexposes the film relative to the surrounding areas where bone is not present. Opacity differences as small as a few percent can be discerned under ideal conditions and high-quality images can be obtained which are an invaluable diagnostic for the medical and the industrial community. X radiography works perfectly well to image materials that do not completely attenuate the beam, that have differences in attenuation (opacity) due to internal structure that the radiographer wishes to study, and that can be oriented perpendicular to the x-ray beam. Consider the problem of producing the radiograph of Mrs. Roentgen's hand when the hand is rotated by 90^{o} relative to the x-ray beam, i.e. thumb toward CRT and little finger toward film. The bones of the fingers would all then coalesce in the image plane and such a radiograph would be virtually useless for producing detailed images of each finger. This is the very problem that tomography was designed to solve: how to render an image of an object in three dimensions so that any arbitrary plane of interest can be displayed when the source and detector or film can not be placed at right angles to the plane of interest. The technique of tomography requires extensive manipulations of large data sets and, therefore, awaited the development of computers. As a benchmark, during the period circa 2000, some analyses could take many minutes to be completed with the speed and data handling capabilities of that time.

Consider Figure 2 which compares the radiographic method with the tomographic method using a pair of concentric metal washers as the sample. The plane of interest, xy, is parallel to the surface of the page and taking a radiograph of the washers with the orientation of beam, sample and film as depicted would be expected to produce a good image of the washers as depicted in the figure. Using tomography, one can reproduce a similar image as depicted in the figure immediately below. The method illustrated here chooses three angles of incidence relative to the two washers (horizontal, vertical and diagonal) and then moves the object (or source and detector) in small steps from one side of the large washer to the other side. In our example, for each of the three angles approximately a dozen measurements or data grabs are made in scanning from one side to the next. At each measurement point, the count rate from the radiation source is recorded by the radiation detector and varies with the inverse of the opacity of the sample along that line of incidence. The resulting count rate is often referred to as a projection or ray-sum.

Figure 3 gives a simple example defining a projection or ray-sum. In this example the sample has been divided up into 10 rows and 11 columns and the 5^{th} row is currently being interrogated with the radiation source and the count rate is inversely proportional to the opacity as defined in the equation at the bottom of the figure. It is clear that the total opacity is simply the sum of the opacities of the different cells making up the 5^{th} row and that the individual opacities are a product of the linear attenuation coefficient and the thickness (ΔX) of the cell.

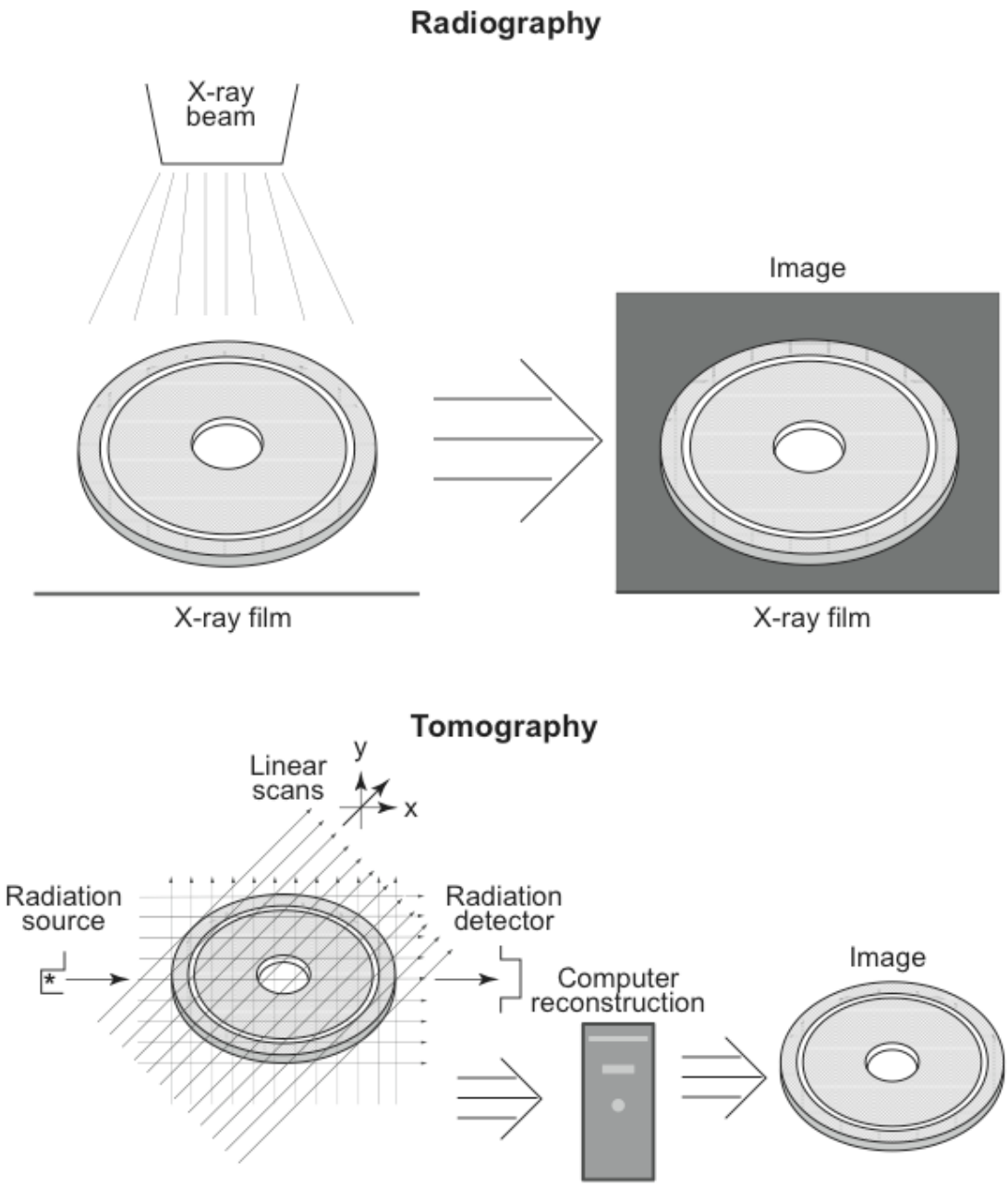

Fig. 2 *Radiography and tomography.*

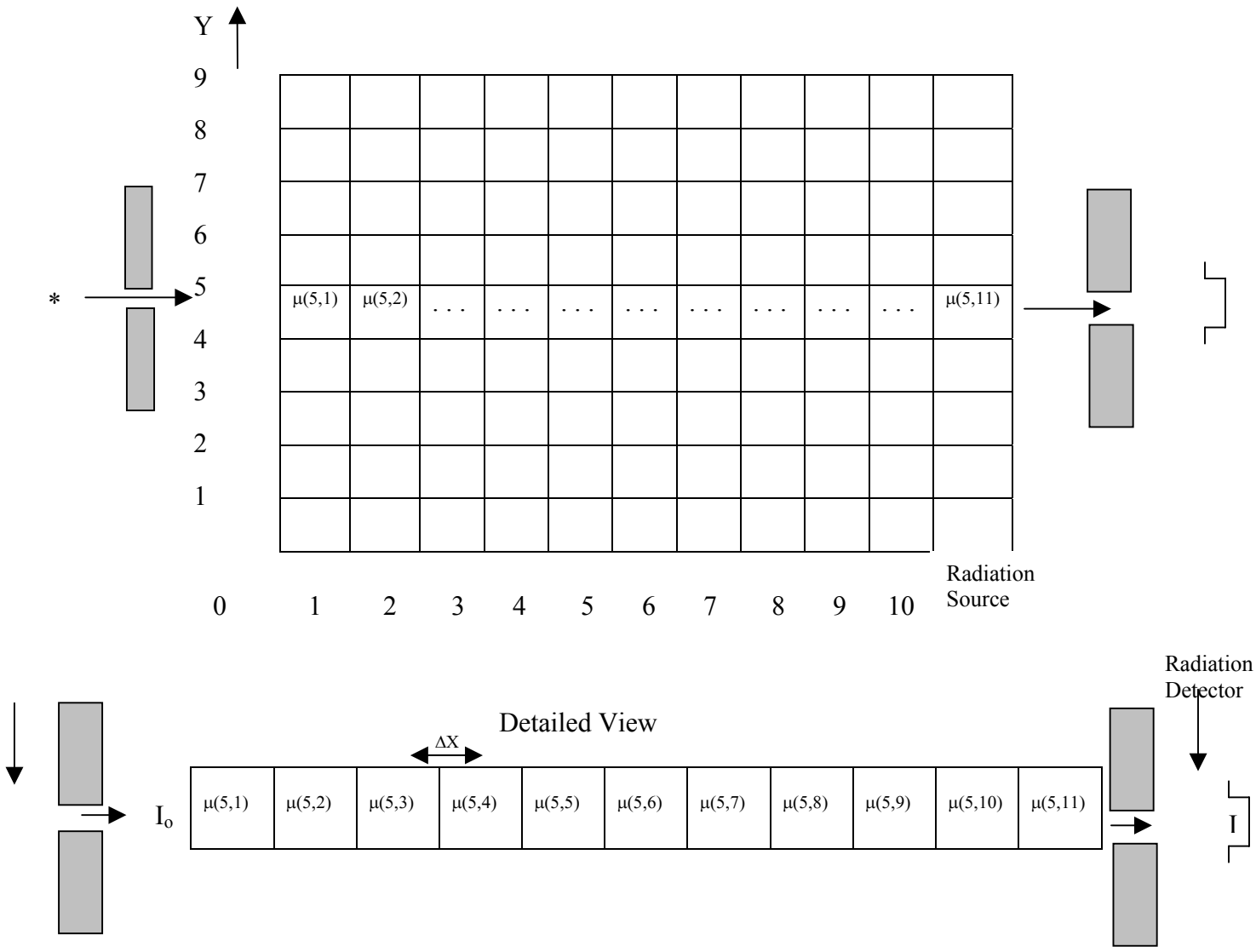

$$I = I_O\, e^{-\left[\mu(5,1)\Delta X_1 + \mu(5,2)\Delta X_1 \ \ldots\ldots\ldots\ldots \mu(5,11)\Delta X_{11}\right]}$$
$$= I_o\, e^{-\left[\mu(5,1) + \mu(5,2) \ldots\ldots\ldots\ldots \mu(5,11)\right]\Delta X}$$

when $\Delta X_1 = \Delta X_2 = \ldots\ldots\ldots\ldots\ldots \Delta X_n = \Delta X$

and the expression below represents the opacity of the 5th row.

$$\left[\mu(5,1) + \mu(5,2) \ldots\ldots\ldots\ldots\ldots \mu(5,11)\right]\Delta X$$

Fig. 3 *Projections or ray-sums are opacity measurements.*

B. Understanding Tomographic Image Reconstruction

Although the detailed algorithms associated with the tomographic image reconstruction from raysums can be complex, the underlying concepts can nevertheless be understood through the study of a set of simple idealized tomographic reconstructions. To this end, we use a very straightforward iterative technique to solve for the opacities of rectangular cells that geometrically define our objects and begin with the 1x1 matrix to demonstrate the rules for this technique. We then successfully apply the same rules to more complex matrices (2x2 and 3x3) and, using mathematical inference, we assume the technique will work for any matrix of arbitrary dimension.

We begin at the top of Figure 4a with the simplest case of tomography, the 1x1 matrix and the "unknown" opacity of this cell has a value of 5. As in Figure 2, we will restrict our data to horizontal, vertical and diagonal projections, whereas in real tomography other projection angles might be used to provide a larger data set. Obviously the horizontal, vertical and diagonal projections will each give a total opacity of 5. Having acquired this data we will blindly follow the rules for image reconstruction given below and compare our estimates with the actual opacity (5) of the cell. This technique we use is a common one called the Algebraic Reconstruction Technique (Ref. 5).

Rules for the Algebraic Reconstruction Technique (ART)

1. Sum and record the actual projections (P^0) for all angles.
2. Make an initial guess at the opacity (O^i) for each of the cells.
3. Calculate the projection for one of the angles for all cells using the latest estimate for the opacities. NOTE: The latest estimate in the case of the first estimate is a guess.
4. Compute each new iteration from the results of the last with the following equation where N is the number of cells in the particular projection under analysis.

$$O^{i+1} = O^i - [P^0 + (P^i - P^0)/N]$$

5. Compare final estimates of the cell opacities once all projections have been applied.

Referring to the 1x1 opacity matrix in Figure 4, our analysis begins with a guess for the initial opacity (O^i) of zero. Even with this poor guess this simple problem immediately converges to the correct result in the first iteration. This of course holds true regardless of the angle of incidence of the projection (horizontal, vertical or diagonal). In Figure 4b, within each cell, the i^{th} opacity is given immediately above the calculated i+1 opacity with a dashed line separating the two values. In general, we have calculated estimates for the cells in the first column of each matrix. The reader may wish to verify our calculations for the remaining cells.

1 x 1 Opacity Matrix Reconstruction Example

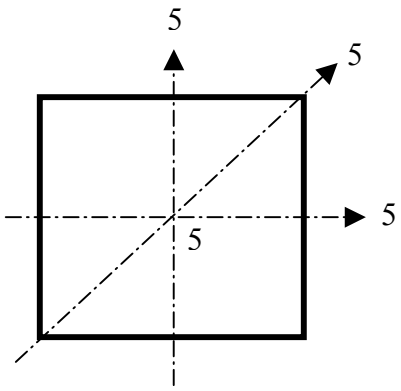

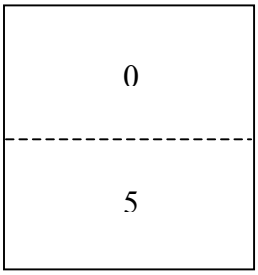

Guess

Estimate = E

For All Projections

$$E = 0 + \frac{[5-0]}{1} = 5$$

Fig. 4a

---

2 x 2 Opacity Matrix Reconstruction Example

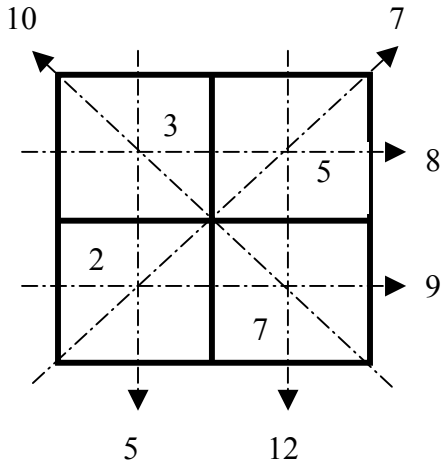

Fig. 4b

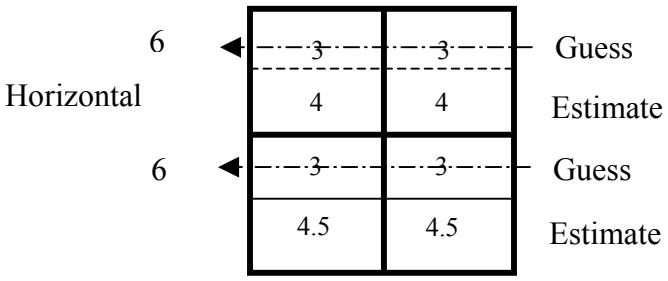

$$E = 3 + \frac{[8-6]}{2} = 4$$

$$E = 3 + \frac{[9-6]}{2} = 4.5$$

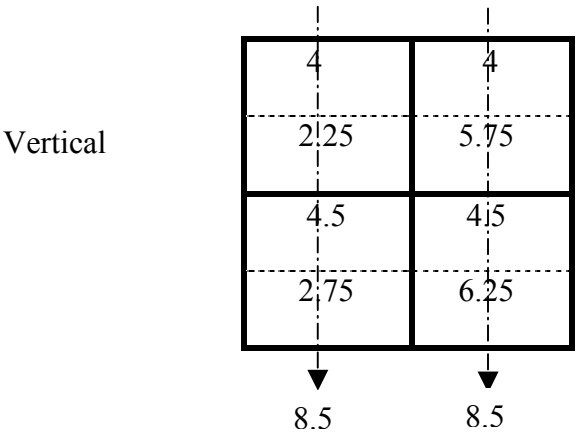

First Column Estimates

$$E = 2.25 + \frac{[10-8.5]}{2} = 3.0$$

$$E = 4.5 + \frac{[5-8.5]}{2} = 2.75$$

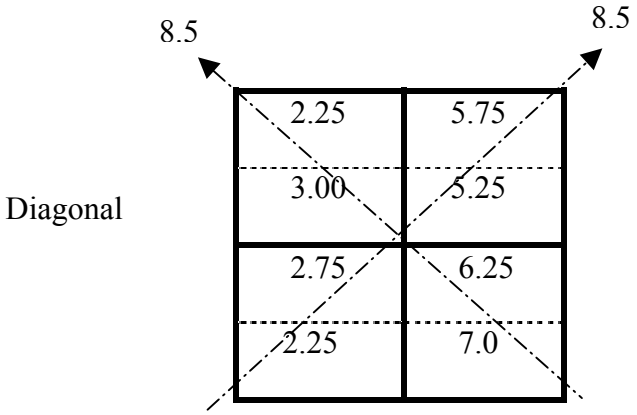

First Column Estimates

$$E = 2.25 + \frac{[10-8.5]}{2} = 3.0$$

$$E = 2.75 + \frac{[7-8.5]}{2} = 2.0$$

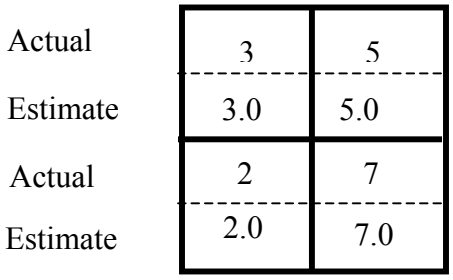

Comparison of Final Estimates with Actual Opacity.

Fig. 4b *continued.*

3 x 3 Opacity Matrix Reconstruction Example

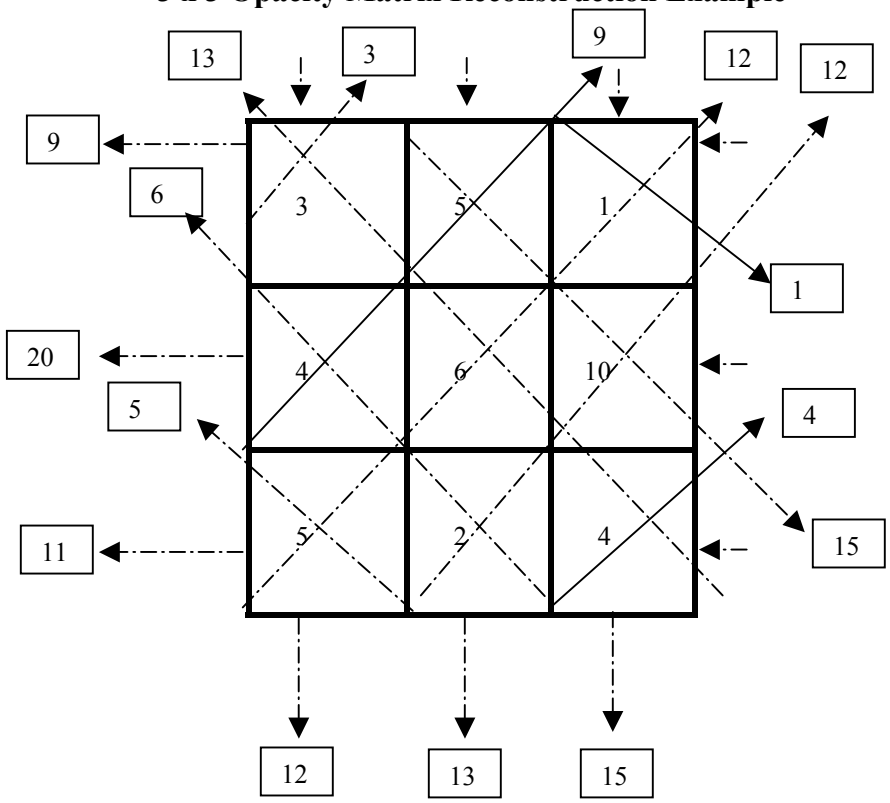

The above are the actual projections or ray-sums.

Preliminary guess and new estimates

First Column Estimate

$$E = 5 + \frac{9-15}{3} = 3$$

$$E = 5 + \frac{20-15}{3} = 6.67$$

$$E = 5 + \frac{11-15}{3} = 3.67$$

Horizontal

Guess	5	5	5
Estimate	3	3	3
Guess	5	5	5
Estimate	6.67	6.67	6.67
Guess	5	5	5
Estimate	3.67	3.67	3.67

Guess	3.0	5.0	1
Estimate	3.04	5.0	1
Guess	4.0	6.0	10.0
Estimate	4.0	6.06	10.0
Guess	5.0	2.0	4.0
Estimate	5.0	2.0	4.04

Final Estimates Compared to Actual Projections

Guess	3		1
Estimate	2.59		3.11
Guess			
Estimate			
Guess	3		4.0
Estimate	2.78		4.26

Results Without Corner Projections

Fig. 4c *The 3 x 3 image reconstruction.*

Having validated our technique for the 1x1 matrix, we now apply it to a 2x2 matrix. Note that after using the four projections for the horizontal and vertical angles of incidence, our estimates for the opacities have improved yet still are rather poor. It is generally the case in tomography that the estimates improve with the number of projections and that exact solutions are rare. Only after applying the diagonal projections to our analysis technique do we find that the technique provides a unique and correct solution, matching exactly the "unknown" opacities. In cases of matrices of larger dimension, even with simple well-defined geometries and cell opacities, unique solutions will generally not exist and final results will depend upon the number of projections and in some cases on the initial guess and the order in which the projections are taken in the analysis. The 3x3 matrix problem illustrates the problems associated with too few projections. We have eliminated the actual calculations for all but the horizontal projections. Beginning with an initial guess of 5 for all cell opacities and proceeding from the horizontal incidence to vertical to left to right diagonal and then right to left diagonal the reader can verify our results at the bottom of Figure 4c. The problem of using too few projections is made clear by comparing the results of the analysis between the two analyses: the first in which we include all of the corner projections and the second where we do not include the corner projections, Figure 4c. The results when the corner projections are not included are very poor and in the case of the upper right corner cell the estimate is in excess of three times the actual opacity.

So in conclusion, we have demonstrated that by using a simple iterative technique, three angles of incidence, and sufficient projections at each of the three angles that very good reconstructions are possible. Thus one might expect for example that by applying our technique to the problem of Figure 2, a reasonable image of the two washers could be produced. This technique was the basis for Computerized Axial Tomography (CAT) scan analysis developed during the 1970's (Refs. 6-9) that led to the Nobel Prize for Medicine in 1979. Such techniques have undergone refinements, but the underlying approach is similar to that applied to our simple problem. In the medical field, such techniques currently provide high accuracy image reproductions at the sub-millimeter level. We have discussed the reproduction of thin slices using tomography. In general, one deals with thick three-dimensional objects and thus one must look at successive slices and combine the results for each of the slices to image a three dimensional object. This will be addressed later in the context of actual TGS measurements.

C. Defining the Geometry

Figure 5 is a schematic of a generic TGS showing the general relationship of the sample, the source, and the high-resolution germanium detector. For a typical one-hour scan of a 208-ℓ drum at each of 10 to 15 axial positions, the drum would rotate at approximately three revolutions per minute while translating in a horizontal direction at approximately 30 cm/min. In Figure 6, the two coordinate systems are shown which are used to uniquely define the motion of the drum. The graph indicates the individual measurement points as a function of the angle of rotation of the drum and the distance the drum has moved from the origin. In a typical ^{239}Pu scan, the drum would start with its outer edge grazed by the collimated beam from the ^{75}Se attenuation-correction source. It would then rotate at 3 rpm while translating to a position where the ^{75}Se beam intersected the radial centerline of the drum. The direction of

translation would then reverse and the drum would return to its initial position. The round trip would take approximately 2 minutes during which time approximately 150 separate data grabs would be acquired. The mathematics relating functions defined within these two coordinate systems was published first by Johann Radon in 1917 (Ref. 10) but went undiscovered through much of the early development of the tomography technique. The idea, nevertheless, is that by means of the Radon transformation a two-dimensional function (such as the opacity as a function of position in the x,y plane) can be inferred from the projections which are defined in terms of an angle of rotation and translation of the object relative to the stationary x,y coordinate system. The drum is then moved vertically approximately 5 cm and the scan is repeated. By stacking sections or slices, one can reproduce a three-dimensional object through superposition. For those who are interested in formulations of a mathematical nature, they are referred to the original article by Radon.

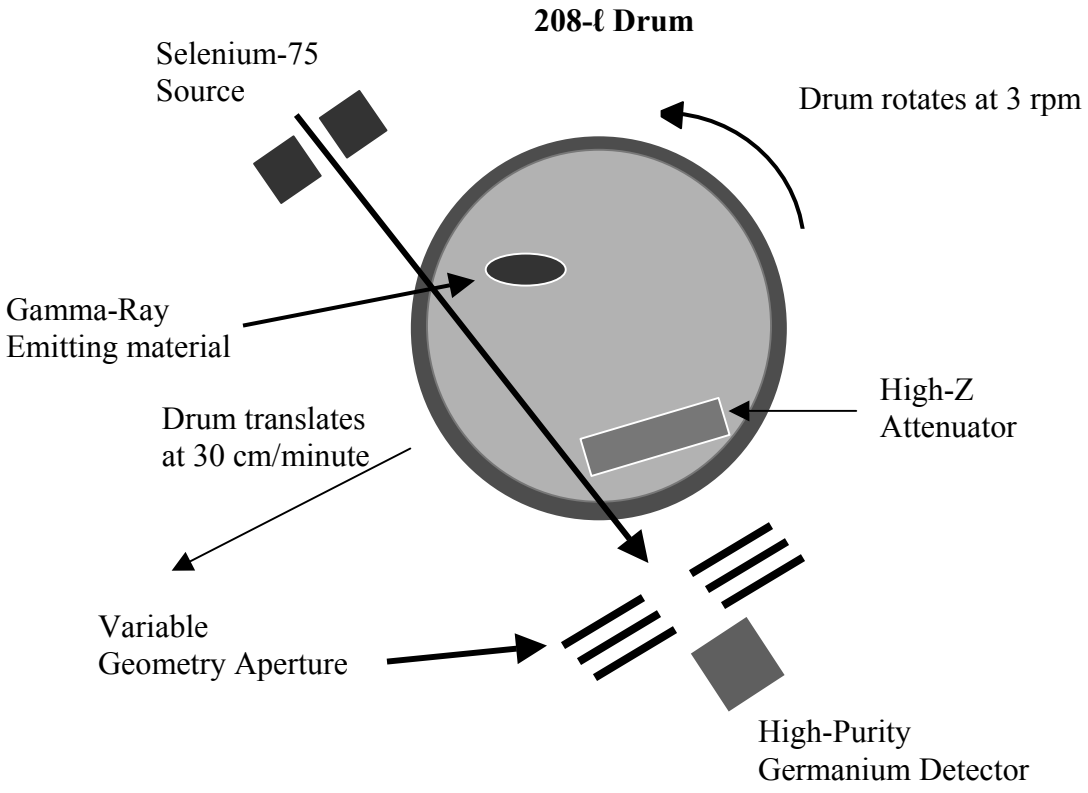

Fig. 5 *The TGS configuration in concept.*

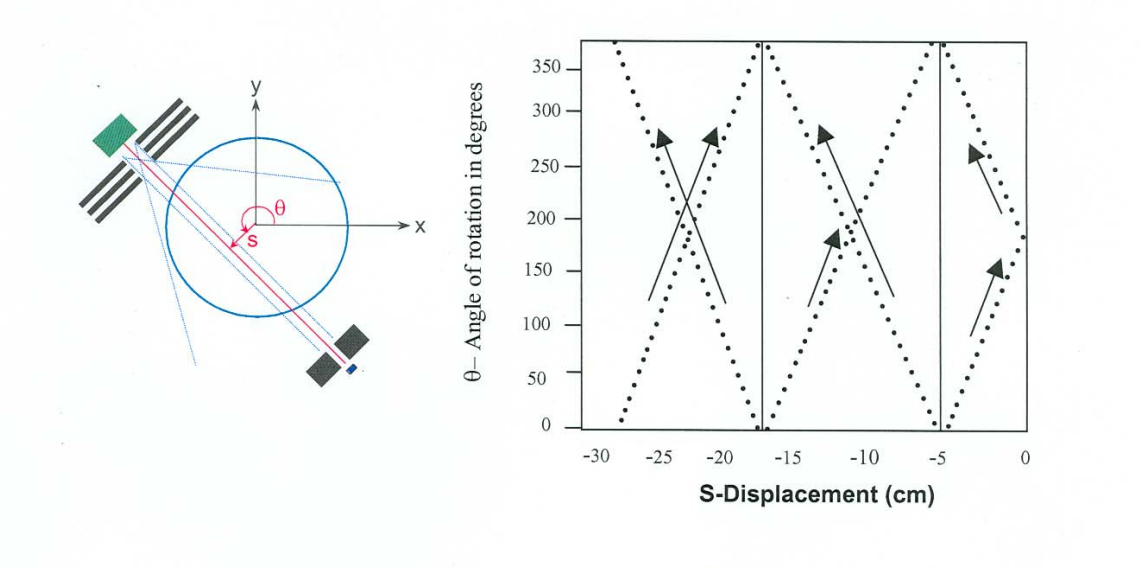

Fig. 6 *The stationary and moving coordinate systems.*

D. Attenuation and Emission Maps

The TGS method counts gamma rays emitted by plutonium or uranium in contiguous small volume elements distributed throughout the sample estimating the mass of SNM from the counting rate of certain characteristic gamma rays. The gamma rays are detected with a high-purity germanium (HPGe) detector and corrections are applied to the count rate for the attenuation by materials intervening between the small volume elements and the detector. The problem of NDA with gamma-ray tomography is one of defining a three-dimensional image of a sample (say a 208-ℓ drum) in terms of a set of three-dimensional "pixels" often termed "voxels" and assigning the appropriate mass of SNM and opacity to each voxel. In effect, the problem is reduced to conducting a gamma-ray assay for each voxel within a 208-ℓ drum. For a 208-ℓ drum divided into approximately 1500 voxels, this corresponds to breaking the problem into an assay of volumes that are roughly 5x5x5 cm^3. By suitable image reconstruction techniques, the result of a tomographic assay is to associate with each of these voxels a mass of SNM and opacity. To estimate the contribution from a particular voxel to the count rate the gamma rays from materials in the voxel are ray-traced to the detector and attenuation corrections are made by summing the opacities of the voxels through which the rays must pass. The image reconstruction of each voxel is involved since the voxels that lie between it and the detector vary as the drum rotates and translates and the germanium detector samples a large volume (many voxels) of the sample, see Figure 6. Nevertheless, by careful geometric definition of the fixed and stationary coordinate systems and the application of efficient reconstruction algorithms, high throughput, low bias, and adequate image reconstruction can be achieved. Having completed the analysis, each voxel is assigned a mass of a specific isotope and an opacity value. Combining the results for each voxel produces a map of the attenuation and another for the emission characteristics of the drum as a function of position (x,y) within the drum. Such maps are shown in Figure 7 for four drums (76 cm high x 61 cm diameter) of varying matrices and ^{235}U mass. The resolution is of the order of a voxel length, 5 cm, and the highest concentration of either matrix material or ^{235}U are indicated by

the color red. The attenuation map is to the left of the emission map for each of the four drums.

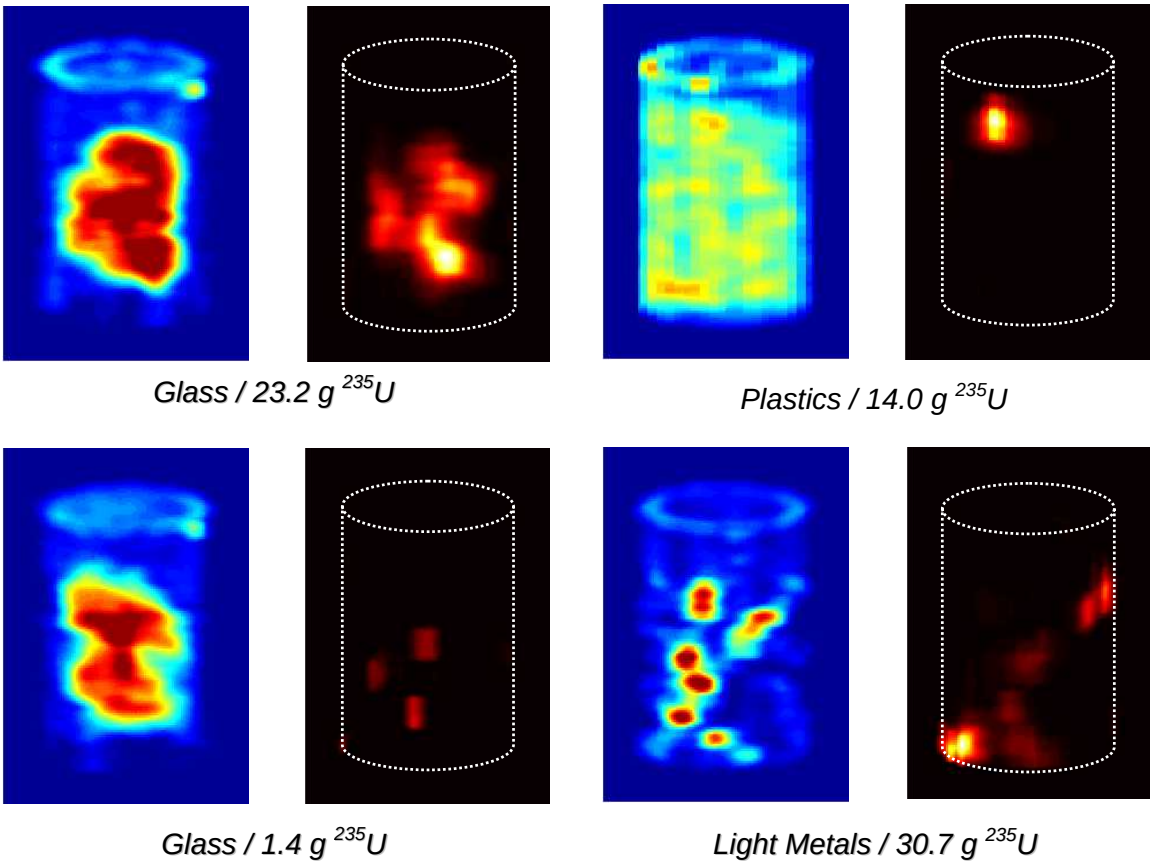

Fig. 7 *Transmission(l) and emission(r) image reconstructions.*

E. Detector Response Function

In medical tomography, high resolution imaging is essential. In the application of tomography to the assay of radiological samples, such as 208-ℓ drums of contaminated waste, throughput is the key issue and high throughput requires large apertures and large germanium detectors. As such, the view and efficiency of such detectors is great and varies for a particular point in space with the inverse of the distance from the detector and to a lesser extent to the degree the point is off the detector axis. It is important to apply these corrections to the detection efficiency and, as a general rule, a detector response curve must be generated for each aperture setting. Figure 8 is the detector response function for an x-axis distance from the detector of 92 cm and a y-axis distance varying from 0 to – 40 cm. At roughly 30 cm, the effects of the tungsten collimator eclipse the source emissions and the count rate falls to zero. Curves such as Figure 8 are normally generated by applying computer models supported by experimental measurements.

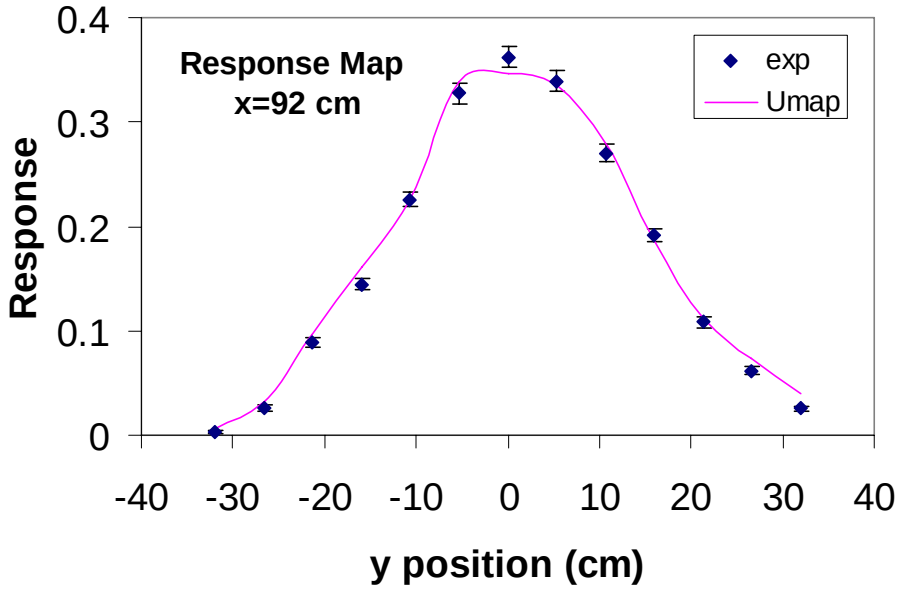

Fig. 8 *Detector response map.*

III. TGS Design Considerations

The design details of TGS systems can vary depending upon the dimensions and weight of the samples to be measured, whether the principal use is in a production environment or in a research laboratory, and to some extent upon the acceptable precision and bias. Versatility, accuracy, and throughput come at a price, but all systems require certain functions or modules to perform. In this section, we will consider the TGS as comprised of these modules and point out some of the design considerations in their selection.

Figure 9 is an engineering drawing for a TGS system fielded from 1998 – 2003 at RFETS (Transportable TGS - TTGS) and the progenitor of the commercial models available through license agreements with Los Alamos National Laboratory. The TTGS was designed for versatility, accuracy, and high throughput in a production environment. In the next section, the results from one of its major assay campaigns is described. It was designed to be very modular and it is well suited for the present discussion. The major modules are the Transmission Source Assembly, the Detector Assembly Module, the Sample Positioning System, the Data Acquisition System, and the Data Analysis Module. Each of these is discussed in turn.

A. Transmission Source assembly

The transmission source is mounted in a tungsten shield on top of a 5.5-m steel tower. A high intensity (30-200 mCi) ^{75}Se source is used to provide high throughput and penetration of dense samples (e.g. cement in 314-ℓ overpacks). Using ^{75}Se for the transmission source, gamma-ray transmission can be measured accurately at several energies (96.7, 121.1, 136.0, 264.6, 279.5, and 400.6 keV) near the important lines of ^{239}Pu and ^{235}U. By interpolating the transmission data, spatial maps of the attenuation coefficient can be accurately obtained at the gamma-ray energies of interest. The only drawback to ^{75}Se is its relatively short half-life (120 days) that

requires sources to be replaced annually. A solenoid-driven tungsten shutter (5-cm thick), when in the open position, provides a tightly collimated beam (0.3-cm diameter) of gamma rays for transmission measurements. For this system, a low-power laser/silicon diode alignment system verifies the alignment of the source and detector. Such enhancements must be considered when systems are to be placed in a rugged production environment.

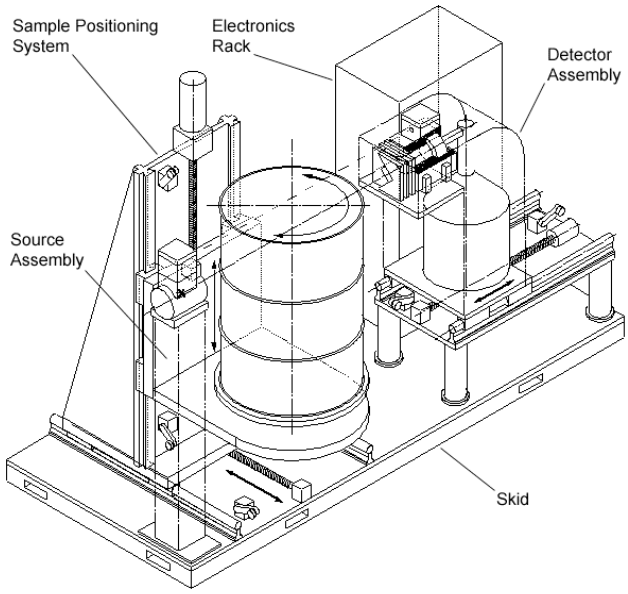

Fig. 9 *RFETS transportable TGS outline drawing.*

B. Detector Assembly

The detector assembly has a HPGe detector, a live-time source (^{109}Cd), a collimator, and shielding. The detector combines high efficiency (> 50%) with high resolution to permit gamma-ray isotopic measurements from the composite spectrum from the emission scans. The opening of the collimator is adjustable by stepping motors from 1.25 cm to 6.4 cm to accommodate a large range of sample sizes. The detector assembly is auto-positioned depending on the sample size selected by the operator. These automated provisions add cost and are not necessary for a research environment or in a production environment in which supervisory oversight can be substituted for automation. For low Pu or U mass measurements in a production environment thick tungsten shields are necessary. The detector is adequately shielded by 10 cm of tungsten.

C. Sample Positioning System

The sample positioning system has a three-axis precision stage driven by stepping motors that provided sample translation, rotation, and elevation relative to the source and detector. Note that the difference between TGS and the older segmented gamma-ray scanner (SGS) is the addition of a translation axis that allows the detector to view the sample along all possible lines that pass through it rather than just through the radial centerline as in the SGS technology. By stacking slices (axial scanning), the spatial distribution of material within the entire sample can be recovered and a three-dimensional mapping of the drum contents is possible. The RFETS system accommodates sample sizes ranging from 15 cm to 75 cm in diameter and up to

908-kg total weight. The largest samples were 303-ℓ drums and the smallest 2-ℓ cans. In a typical transmission scan of a 208-ℓ drum, the drum rotates at 3 rpm, makes 5 entire revolutions, and takes 150 data grabs of the entire spectrum for each axial layer. The total transmission scan of 16 layers takes 30 min and then the stage and drum return to the initial position, the shutter is closed, and the scan protocol is repeated with a high degree of repeatability (< 0.013 cm).

D. Data Acquisition System

High throughput and accurate, unbiased results are the hallmark of a well-designed TGS system. Current data acquisition systems, if well specified, should not be the limiting factor. General requirements might include grabbing and storing 5000 measurements per hour with individual grab times of approximately 2/3 s. Each measurement is associated with a particular projection as depicted in Figure 6. Summing these measurements provides an average spectrum suitable for post-scan isotopic abundance determinations.

E. Data Analysis System

During the emission scan, the transmission source shuttered off and net counts are recorded for regions of interest (ROI) about peaks corresponding to gamma rays emitted by the target isotope. For plutonium assays, ROIs are typically established for four well-resolved ^{239}Pu gamma rays: 129-, 203-, 345-, and 414-keV. Each of these gamma rays is used to develop an independent estimate of the distribution and mass of ^{239}Pu within the sample. When large variations are observed for the different energy estimates, the presence of self-attenuating lumps is indicated and lump correction algorithms must be applied. (See Section VI.) As the sample rotates and translates relative to the detector, the net count rate varies. The magnitude of the net count rate depends on the distance from the gamma-ray source to the detector, and the intervening attenuating material. Since the attenuation map is known for each gamma ray of interest, the net count rate can be calculated for trial distributions of the emitting material. Reconstruction of this spatial distribution of emitting material is accomplished by adjusting the trial distribution until the estimated net counts match the measurements (Refs. 6-7). The exact nature of such algorithms depends upon the approaches devised by the developers. The reader is referred to the following references which provide insight into the approaches used successfully by leading TGS designers (Refs. 12-18).

IV. Performance Evaluation in Blind Tests and Actual Facility Measurements

A major selling point of TGS has been its overall versatility and freedom from bias. In this section, we will present a small but representative set of results to help the reader evaluate the TGS approach. The first data set is from the Performance Demonstration Program (PDP) comparing TGS to a large number of competing technologies in controlled blind tests. The second and third set of results are from large production runs for classes of materials that are very difficult to assay by any technique other than TGS and validate the time and effort invested to develop the technology.

A. Performance Demonstration Program (PDP)

"The Performance Demonstration Program (PDP) for NDA consists of a series of tests to evaluate the capability for NDA of Transuranic waste (TRU) throughout the DOE complex with the major interest relating to TRU waste to be shipped for storage in the Waste Isolation Pilot Project (WIPP) in Carlsbad, NM. Each test is termed a PDP cycle. These evaluation cycles provide an objective measure of the reliability of measurements obtained from NDA systems used to characterize the radiological constituents of TRU waste."(Ref. 19)

The test results given in Figure 10 are from a series of blind tests of 208-ℓ drums of a known matrix (glass, plastic, sludge, etc) and an unknown distribution and mass of the target isotopes. Radioisotope concentrations for the set of tests were varied over a range expected in actual waste characterization activities. Measurement facilities were required to analyze the simulated waste containers using the same procedures used for normal waste characterization activities. The results are mixed and no single measurement performs better than all others for all situations. The reader is allowed to draw their own conclusions but is referred to the TGS Applications Manual (Ref. 4) that provides more details about these series of tests.

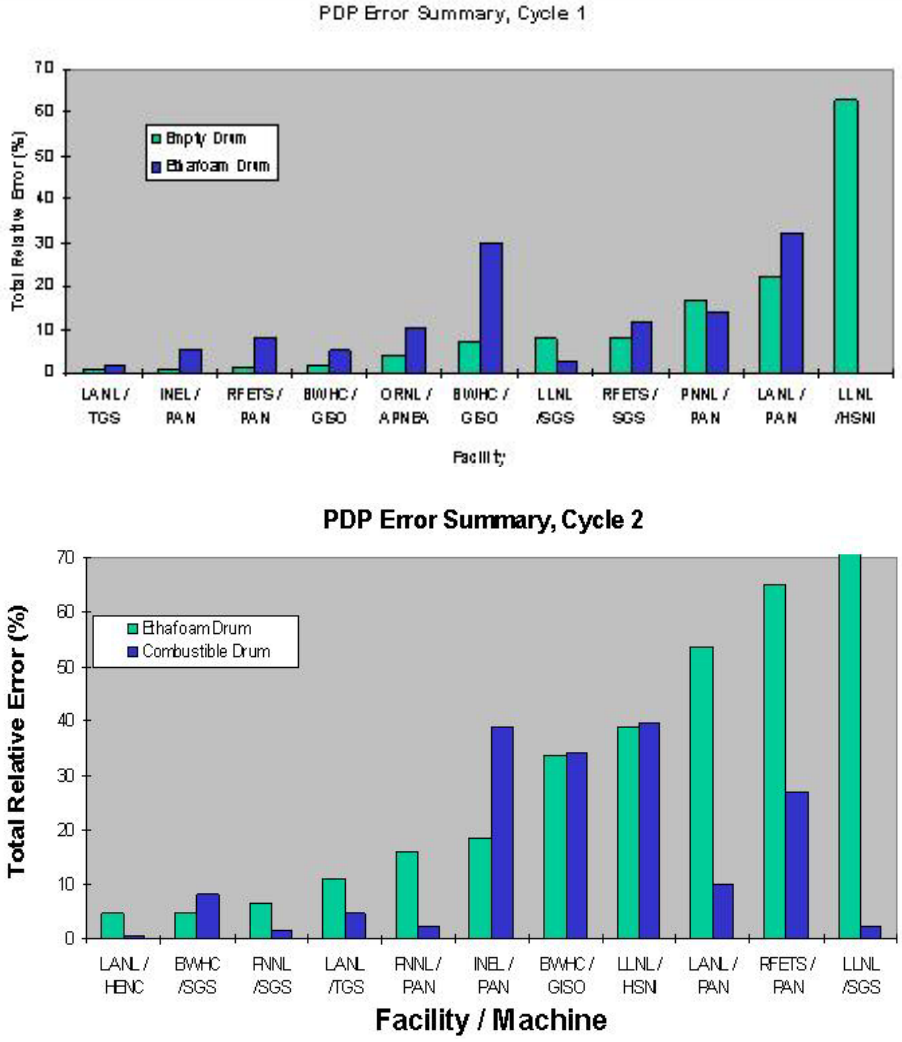

Fig. 10 *PDP results*

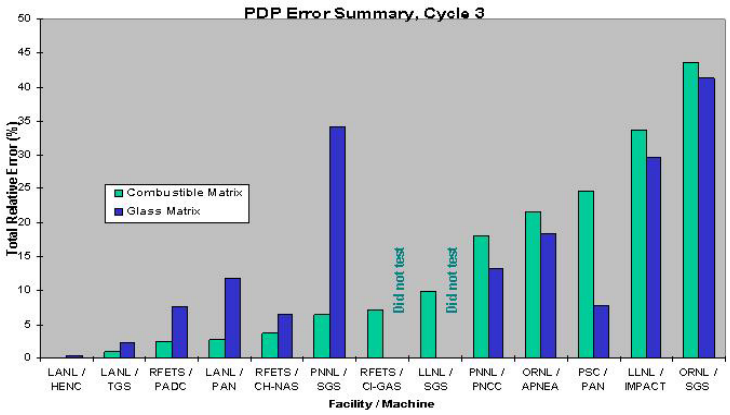

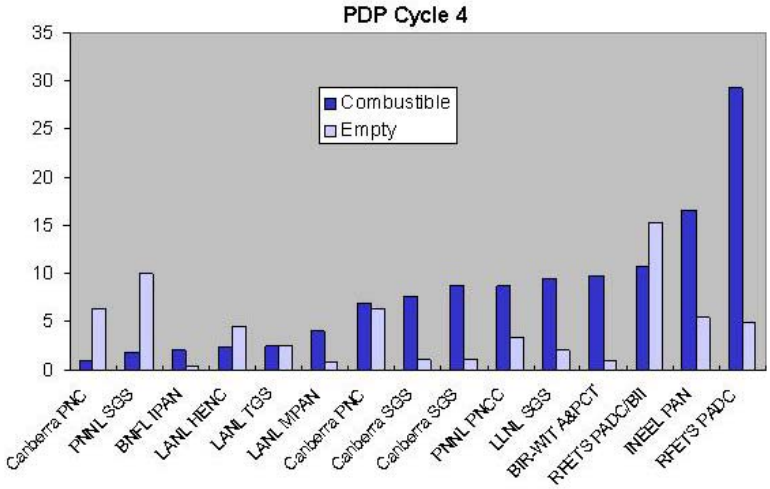

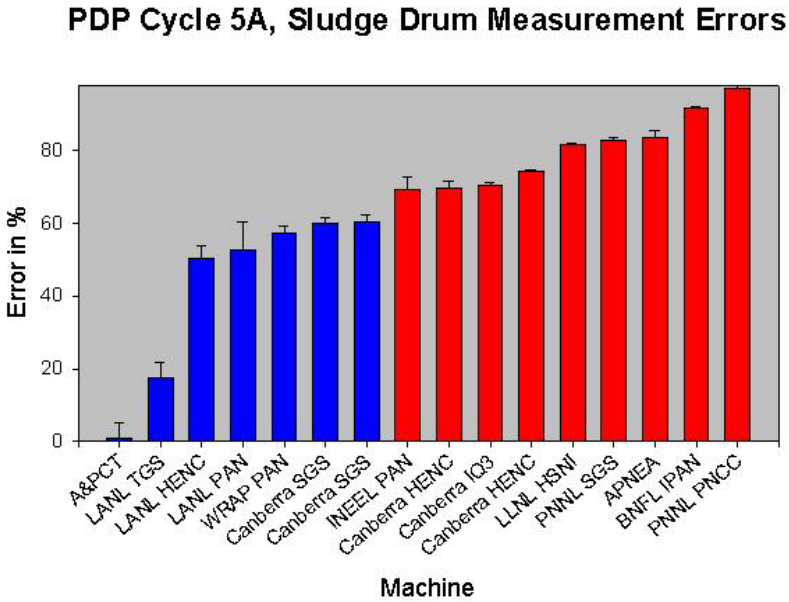

Fig. 10 *PDP results (continued).*

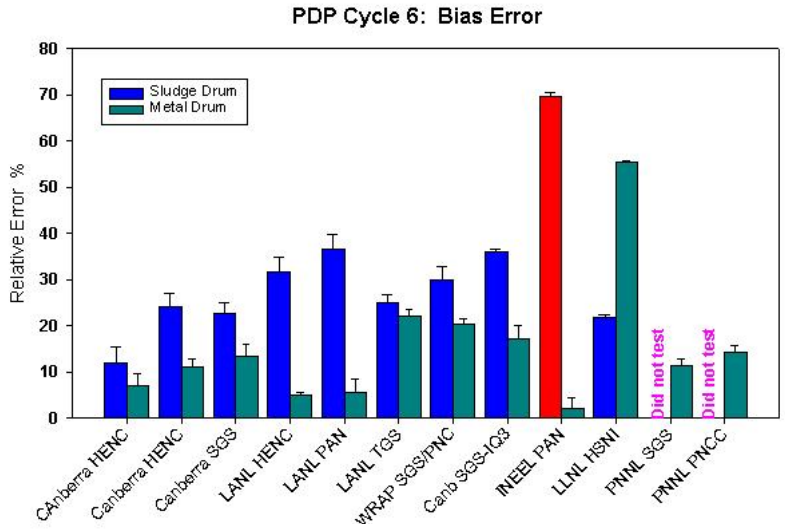

Fig. 10. PDP results (continued)

Figure 10 PDP Results Legend

Facilities: INEEL – Idaho National Engineering and Environmental Laboratory, RFETS – Rocky Flats Environmental Technology Site, SRS – Savannah River Site, WRAP – Hanford Waste Receiving and Packaging Facility, LANL – Los Alamos National Laboratory, LLNL – Lawrence Livermore National Laboratory, ORNL – Oak Ridge National Laboratory, PNNL – Pacific Northwest National Laboratory

Instrument: HENC – High Efficiency Neutron Counter (passive drum counter), SGS – Segmented Gamma Scanner, PAN – Passive Active Neutron Counter, IPAN – Imaging Passive Active Neutron Counter, TGS – Tomographic Gamma Scanner, CTEN – Combined Thermal Epithermal Neutron Counter (Active/passive counter), IQ3 – Low-level sensitivity Multi-detector gamma counter, A&PCT – Active and Passive Computed Tomography, APNEA - Active and Passive Neutron Examination and Assay System, PADC - Passive Active Drum Counter, PNCC – Passive Neutron Coincidence Counter, HSNI- High Sensitivity Neutron Instrument

B. RFETS Pyrochemical Salts

The transportable TGS was installed in Building 371 at RFETS for use in the salt repackaging program. Before the start of operations, the system demonstrated compliance with safeguards and WIPP requirements (Refs. 20-21). The system was calibrated using SGS standards. To assess the accuracy of the system, assays of electro-refining salts were compared to reference values determined by calorimetry. For each sample, the mass of ^{239}Pu was determined using TGS with lump corrections. FRAM was used to analyze the spectrum acquired by the DSPEC (commercial multichannel analyzer using direct signal processing) system during the TGS emission scan. The ^{239}Pu/Pu ratio calculated by FRAM was used with the TGS estimate of ^{239}Pu mass to determine total Pu. The results of this procedure are compared to the reference values in Table 1. The mean absolute difference between TGS and

calorimetric assay was 4.5%. The inventory difference was 2.6% (48 g out of a total of 1839 g). Based on the results of these measurements, TGS was qualified to measure electro-refining salt samples in the 25-225 gram range and began routine operation.

. Table 1. Comparison between TGS and calorimetric assay of electro-refining salts

	Calorimetric Assay	TGS/FRAM	Difference
Sample ID	Total Pu (g)	Total Pu (g)	(%)
Z10783	45.07	44.6	-1
Z10671	142.6	151	6
Z10668	186.6	184	-1
Z10626	194.0	200	3
Z10636	151.8	160	5
Z10637	171.7	196	14
Z10639	204.5	200	-2
Z10649	162.5	161	-1
Z10731	97.26	92	-5
Z10762	130.8	128	-2
Z10765	121.8	131	8
Z10781	80.63	83.2	3
Z10782	62.36	63.6	2
Z11395	87.43	92.5	6
Total	1839	1887	2.6%

Pyrochemical salts contain plutonium dissolved in NaCl as well as plutonium in the form of metal shot. These residues also contain high concentrations of ^{241}Am and other radioactive contaminants. Because the salts are highly inhomogeneous, the established SGS technique, which is based upon homogeneity within segments, could not meet the WIPP criteria for accuracy and bias. Calorimetric techniques are capable of giving reliable results, but throughput is very low requiring an average of 20 hours per package. NDA techniques based upon neutron coincidence counting were unable to provide reliable results because of the inability to establish standards for the wide range of impurities and high ^{241}Am concentrations that produced a high singles background. As such TGS was applied to the problem materials and the measurement control results are shown in Figure 11.

The low bias (0.04%) and the high throughput (10 – 20 packages per day) are very notable. The background in the radiation area was significant and demonstrated the advantage of the heavy shielding, described in Section III. Some of the packages were encased in a tin liner which strongly absorbed the emissions and increased the difficulty of the measurements. Below are provided some general guidelines that apply to the measurement of plutonium.

Performance results depend both on sample size and material density and the product of these terms that is called the areal density [g/cm^2] which is often used to express material "thickness" limitations. As a rule-of-thumb, TGS measurements of ^{239}Pu using the 414-keV gamma ray generally have better than 10% accuracy for samples with an areal density less than 90 g/cm^2 assuming the materials are relatively low atomic number.

Transportable TGS Measurement of Salts (1999-2000)

Results from 209 verification runs →

•Uncertainty per meas. = 9.4%

•Inventory Bias = (-0.04 ±0.99)%
13.461 kg (TGS)
13.467 kg (Cal/Iso)

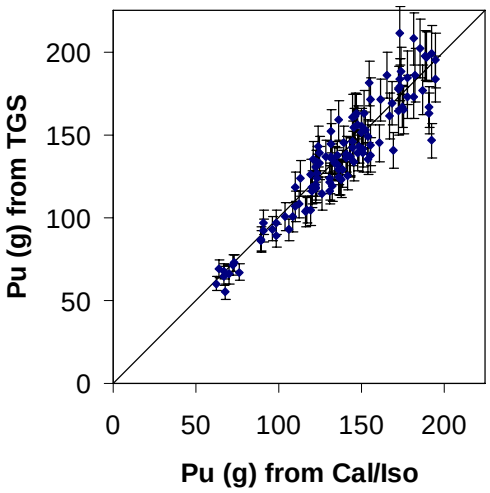

Throughput:

>5000 items / first year

10-20 items / day

Fig. 11 *Results of electro-refining salts assay at RFETS (Ref. 22). Cal/Iso is the combination of a calorimetric determination of sample power (heat) and a gamma-ray spectrometric determination of plutonium isotopic composition.*

For typical salt cans, approximately 20 cm in diameter, 10 % assays can be achieved at bulk densities of 4.5 g/cm^3. TGS is capable of accurately assaying samples that contain regions far exceeding these bulk densities so these estimates tend to be conservative. The precision that can be achieved by TGS varies from sample to sample and depends on the placement of the source, the distribution of attenuating material, collimator parameters, and the mass of SNM present in the sample. As a general rule, 0.5 g ^{239}Pu in low-density matrices with less than one-hour acquisition time is a mass limit below which measurements become unreliable (Ref. 23). For small mass samples (< 5 g) known to be homogeneous, SGS can produce the equivalent precision of TGS with shorter counting times. For example, for a 1-g sample and typical collimator settings, a 20-min SGS scan produces the same precision as a 1-h TGS scan. For samples less than 10 g ^{239}Pu, precision differences are not a significant issue and the presence of any sample heterogeneity will generally lead to more favorable TGS results.

C. Uranium Applications

1. RFETS Experience

TGS was primarily developed to assay plutonium in difficult matrices. In June 1997, TGS was deployed in Building 886 at RFETS to assay 208-ℓ drums containing waste contaminated with highly enriched uranium, HEU (Ref. 24). In this case, the materials were contaminated with solutions containing uranium and other elements including boron. The boron biased the active neutron measurements and the HEU had too little neutron output for passive

measurements. Inhomogeneities ruled out SGS and the very low heat output precluded calorimetry. The materials were primarily contaminated with uranyl-nitrate solutions and consisted of low-Z matrices of borosilicate glass, paper, plastics, cardboard, light metals, soil, and chemical waste all packaged in 208-ℓ drums. The mass of ^{235}U ranged from less than 5 g in approximately 80% of the drums to 60 g in a few cases. All of the drums with assay values less than 15 g were shipped offsite for burial. Those with greater assay values were repackaged using the TGS images to facilitate the repackaging. The lower measurement limit was approximately 0.5 g ^{235}U for the low density matrices. This work was important in providing evidence that the TGS technology applies to a wide collection of uranium items that are difficult or impossible to assay by any means.

2. Survey of Excess HEU Materials across the DOE Complex (Refs. 25-26)

Because uranium assay is not yet as widely done as plutonium assay, some general information is provided here to assist the reader in assessing the use of TGS for uranium assay. The following table indicates the amounts of uranium at various sites across the DOE complex.

Table 2. Excess HEU at DOE Sites

Facility	Excess Uranium (Tonnes)
Idaho	23.0
Pantex	17.0
Portsmouth	22.0
Oak Ridge	85.0
Savannah River	5.0
Total	174.0

Table 3. Excess HEU Material Forms at DOE Sites

Material Form	Excess Uranium (Tonnes)
Metal	87.0
Irradiated fuels/targets	29.6
Compounds	17.4
Reactor Fuel	19.1
Oxide	15.7
Other	5.2
Total	174.0

3. Relative Comparison of TGS Measurements of HEU and Pu (Ref. 27)

The safeguards community has gained considerable background in the TGS measurement of plutonium in a variety of matrices. It is not generally recognized that uranium is also well suited for TGS measurements. To facilitate the readers' appreciation for the ability of TGS to handle uranium contaminated materials, a quantitative comparison of the assay expectations is made below between HEU and plutonium for a typical assay geometry. The tables are based on the assay of 208-ℓ drums observed by a 50% efficient Ge detector. It is assumed that the

attenuating material at a thickness equivalent to half the drum diameter and at the specified Z, is sufficient to reduce the 414-keV gamma ray of ^{239}Pu by a factor of 100. This condition sets a conservative upper limit on the matrix density, corresponding to a factor of 10^4 reduction in the transmission at 414 keV, which challenges the effective dynamic range of typical Ge detectors. For convenience, the count rate at 414 keV, given this reduction, is taken to be 1 count/s. Under these same conditions, the identical matrix would reduce the 186-keV gamma ray from ^{235}U to the count rates given in Table 4a,b. It is important to note that in the absence of any attenuating matrix whatsoever, the count rate per gram would actually be greater for ^{235}U than for ^{239}Pu by a factor of approximately 2.5. This results from the higher specific activity of ^{235}U [4.34 x 10^4 γ/(s-g) at 185.7 keV] versus ^{239}Pu [3.42 x 10^4 γ/(s-g) at 413.7 keV] and the higher intrinsic detector efficiency at 186 keV than at 414 keV (approximately a factor of 2).

The conclusion that one can draw from this comparison is that for conditions conducive to ^{239}Pu assay, i.e. in matrices that produce an average attenuation of less than a factor of 100 and in matrices that consist of materials such as graphite, combustibles, oxides, fluorides, sludges and ash, the count rate per gram for uranium should be comparable to that of plutonium. It is equally important to realize that when the matrix contains elements with Z greater than 20, the low energy of the principal assay line in uranium (186 keV) strongly limits the application compared to plutonium which uses the 414-keV line which is less attenuated.

Table 4a. Excellent Candidates for TGS Assay

Isotope	Plastics, Graphite Molds Combustibles, Raschig Rings Z=6		Oxides, Fluorides Z=8,9		Light Metals Soil, Dirt, Sludge Z=13,14		Steel, Iron Z=26	
	μ[cm2/gm]	count/s	μ[cm2/gm]	count/s	μ[cm2/gm]	count/s	μ[cm2/gm]	count/s
^{239}Pu (414 keV)	0.094	1.0	0.094	1.0	0.094	1.0	0.091	1.0
^{235}U (186 keV)	0.125	0.55	0.125	0.55	0.127	0.50	0.145	0.16
Counting Ratio (Pu/U)		1.8		1.8		2.0		6.3

Table 4b. Poor Candidates for TGS Assay

	Medium Z (Tin, Cadmium, Salts) Z=50		Heavy Metals Pb, W, U, Pu Z=82	
	μ[cm2/gm]	count/s	μ[cm2/gm]	count/s
^{239}Pu	0.105	1.0	0.203	1.0
^{235}U	0.351	$7x10^{-5}$	1.13	$2.5x10^{-9}$
Counting Ratio (Pu/U)		1.4×10^4		4×10^8

Owing to this major difference in attenuation as the atomic number of the absorber increases, self-attenuation in uranium presents an especially difficult problem. The next section discusses the problems of lump detection and correction in plutonium and the success that developers have had in inventing techniques for treating the problem that eliminates bias due to self-attenuation. It has been generally recognized by experts that application of the standard plutonium lump detection and correction techniques to uranium does not lead to the same success as in plutonium. In the absence of another technique for lump detection, one must rely entirely on knowledge that the materials are free of lumps to avoid large negative biases. We suggest here an alternative approach for uranium lump detection and correction that may provide the necessary assurance that materials with uranium lumps can be easily detected and appropriate corrections applied. The study is in a very preliminary phase, but the relative simplicity of the approach shows sufficient promise to allow those who are contemplating the assay of uranium materials the opportunity to test out the preliminary assumptions.

V. Lump Correction Techniques

A. Plutonium Lump Detection and Correction Technique

An important aspect of minimizing bias in TGS measurements is to identify the presence of small lumps of plutonium and apply suitable corrections for the self-attenuation of the gamma rays from these lumps. The self-attenuation in spherical lumps is formulated in Ref. 29. Even small lumps can cause significant bias, e.g., a plutonium metal lump of only 2-mm diameter attenuates 70% of the 414-keV gamma rays emitted within it.

An approach to lump detection and correction has been developed and applied successfully for the assay of plutonium-bearing materials (Refs. 29-31). This approach involves dividing the sample into a homogeneous fraction and a "lumpy" fraction and then estimating the average plutonium lump size using the reduced count rates of lower energy ^{239}Pu peaks relative to the main 414-keV peak. A convenient means for displaying this technique is shown in Figure 12. The idea here is to estimate the mass of the plutonium in the sample using each of the high intensity lines of ^{239}Pu ignoring the effects of self-attenuation. In the presence of lumps, the low energy lines grossly underestimate the plutonium mass and by extrapolation of the mass estimates as a function of gamma-ray energy to 414 keV and beyond a corrected mass is found.

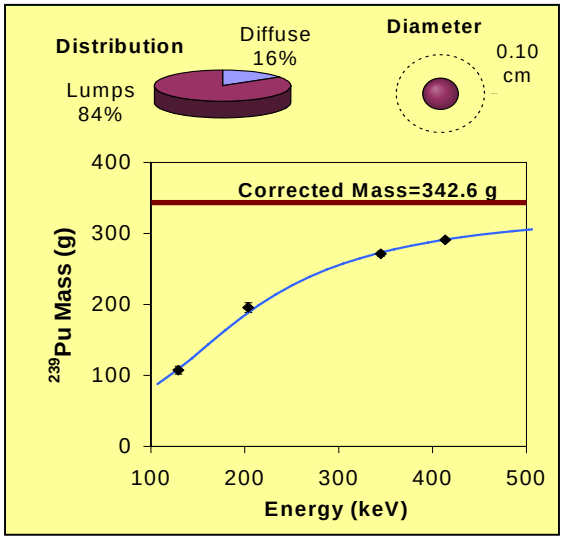

Fig. 12 *Lump Correction estimate of the mass of plutonium metal in a sample.*

B. Standard Pu Lump Correction Doesn't Work for Uranium

The success of this method for ^{239}Pu derives from the high specific activities of the lower energy gamma rays (in particular at 129 keV) and the large change in the attenuation coefficient over this energy range. Uranium poses a special problem because the only line of high intensity is relatively low in energy (186 keV) and the other lines are close in energy and have a much smaller range of attenuation coefficients. To acquire a quantitative feel for the problem, it is instructive to compare the gamma rays used for ^{239}Pu and the corresponding attenuation coefficients in the metal with the corresponding gamma rays of ^{235}U. Table 5 gives this comparison. The ratio of the attenuation coefficients at 129.3 keV and 413.7 keV is 13.8 which compares to a ratio of 1.87 for 143.8 keV and 185.7 keV of uranium. The low intensity of the 205.3-keV and 163.4-keV gamma rays of uranium (factor of 10 less than the 185.7 virtually eliminate them from being useful in a lump correction method as applied above for ^{239}Pu. Because of these large differences in sensitivity, the Pu technique described above is not feasible for uranium and a new approach has been proposed (Ref. 28) as is outlined in the following section.

Table 5. Comparing the relative intensity and attenuation coefficients of U and Pu for possible "lump detection gammas".

Plutonium			Uranium		
E (keV)	γ/(sec-gm)	μ [cm^2.gm]	E (keV)	γ/(sec-gm)	μ [cm^2.gm]
129.3	1.44×10^5	3.714	143.8	7.8×10^3	2.737
203.5	1.28×10^4	1.259	163.4	3.7×10^3	2.003
345.0	1.28×10^4	0.386	185.7	4.3×10^4	1.463
413.7	3.42×10^4	0.269	205.3	4.0×10^3	1.333

C. Proposed Technique for Uranium Lump Correction

This technique compares the self-fluorescence of the uranium K x-rays to the thorium K x-rays produced in the decay of ^{235}U as shown in Figure 13. The upper spectrum comes from a thick uranium metal disk, whereas the lower spectrum comes from two very thin uranium metal disks (~0.03 mm). The $K_{\alpha 1}$ and $K_{\alpha 2}$ x-rays from uranium are at 98.4 and 94.7 keV, respectively. They are the upper two green peaks in the spectra. The corresponding thorium x-rays are at 93.4 and 90.0 keV; they are the lower two green peaks. Note that for the thin foil, where we expect relatively little fluorescence, the ratio of the U x-ray activity to Th x-ray activity is almost one. On the other hand, the same ratio for the thick disk in the upper spectrum, where we expect more fluorescence, is much higher. The thin foil case corresponds to "no lumps" and the thick disk case corresponds to "lumps".

A quantitative comparison, given in Table 6, helps one appreciate the potential sensitivity of this proposed method to correct for "lumps" in uranium measurements.

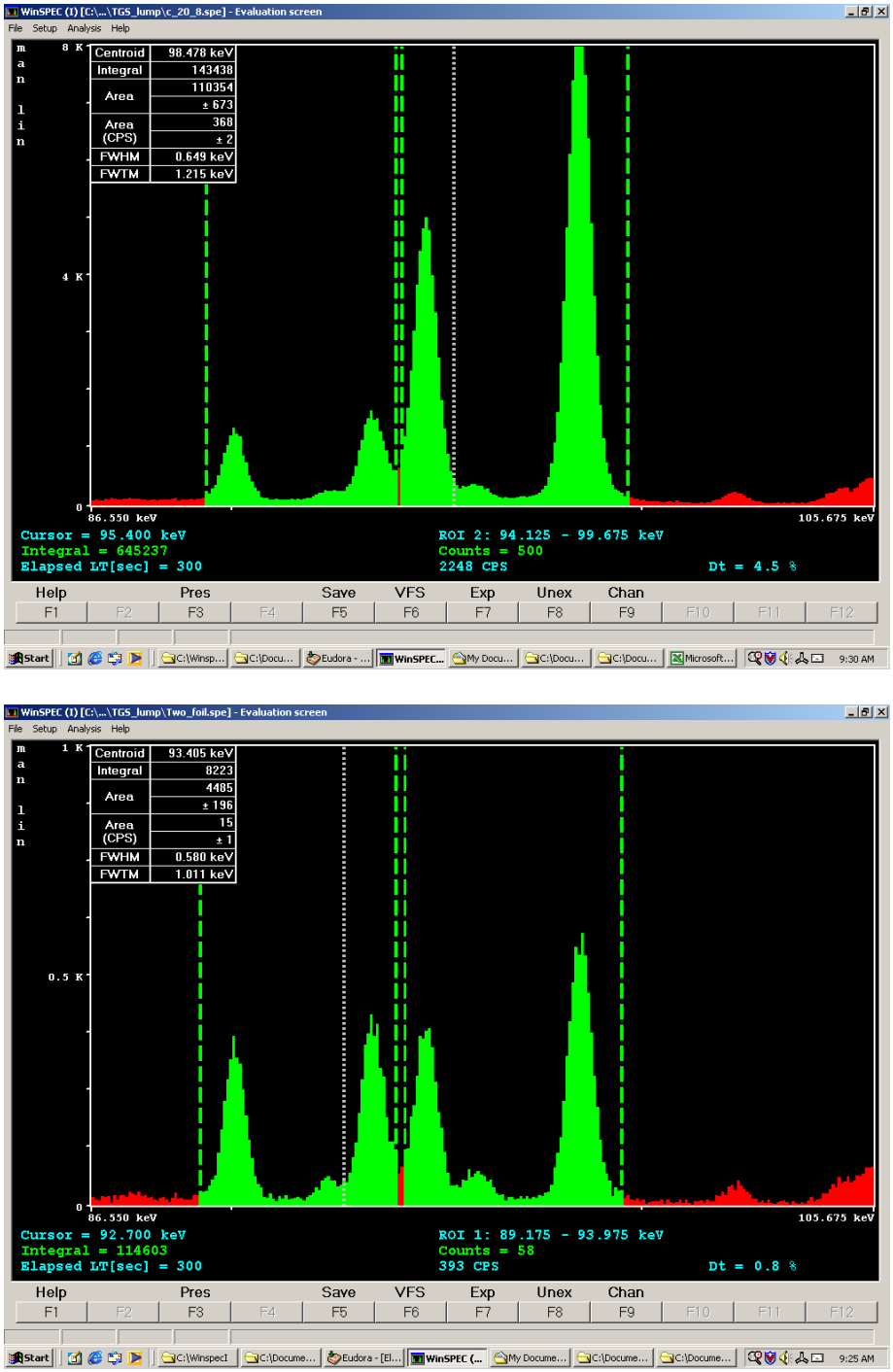

Fig. 13 *Comparison of the fluoresced uranium K x-rays with thorium K x-rays (from U decay) in a thick metal disk (upper spectrum) with those from very thin foils (lower spectrum). The lower energy ROI covers the Th Kα x-rays and the higher energy ROI covers the U Kα x-rays. Note the much higher relative intensity of the uranium x-rays from the metal disk.*

.

Table 6. Comparison of the peak areas of the fluoresced uranium x-rays in thick versus thin samples of ^{235}U

X Ray Group	Metal Disc	Two Foils
Uranium	110354	6141
Thorium	6141	4485
Ratio	18/1	1.4/1

The important fact to note in the above table is that a factor exceeding ten is observed in the ratio for thin versus thick samples, e.g. uranium solutions versus large lumps. This large factor tends to suggest excellent sensitivity to the presence of lumps and with a more careful study even a means of correcting for their presence. As the DOE complex becomes more focused on the uranium assay problem, this technique may become standardized as a means of screening uranium materials suited for TGS assay.

VI. Commercially Available Systems

With the success of the LANL developed TGS systems at RFETS, the technology was validated and license agreements negotiated with the following firms:

Antec Corporation
9076 Marshall Court
Westminster, CO 80031

BNFL Instruments
4001 Office Court Drive, No. 800
Santa Fe, NM 87505

Ametek Ortec
801 South Illinois Ave
Oak Ridge, TN 37830

Figure 14 shows two instruments that are currently available and fielded at several DOE sites.

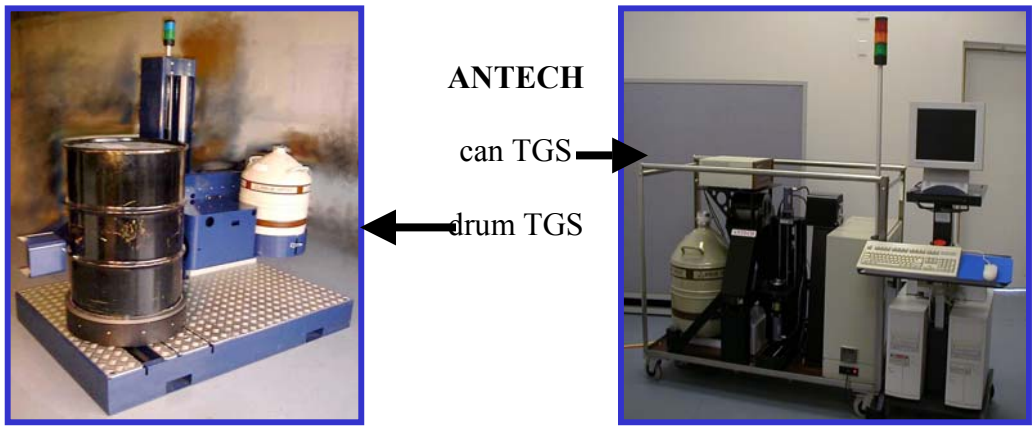

Fig. 14 *Commercially available TGS systems.*

References:

1. R. J. Estep, “Assay of Heterogeneous Radioactive Wastes by Low-Resolution Tomographic Gamma Scanning”, ANS Transactions **62**, 178 (1990)

2. S. Kawasaki, et. al. “Radioactivity Measurement of Drum Package Waste by a Computed Tomography Technique” Applied Radiation and Isotopes **41,** 983(1990)

3. R. J. Estep, and K. Sherwood, “A Prototype Tomographic Gamma Scanner for Assaying 208-liter drums” Los Alamos National Laboratory report, LA-UR-91-61 (1991).

4. J. S. Hansen et. al. “Applications Guide to Tomographic Gamma Scanning” To be published, 2004.

5. R. Gordon, “A Tutorial on Algebraic Reconstruction Techniques (ART)” IEEE Transactions **NS-21** 78 ff. (1974)

6. R. Gordon, R. Bender, and G. Herman, "Algebraic reconstruction techniques(ART) for three dimensional electron microscopy and X-ray photography," Journal of Theoretical Biology **36**,105-117, 1970.

7. G. Hounsfield, "A method of an apparatus for examination of a body by radiation such as x-ray or gamma radiation," Patent specification 1283915, The Patent Office, 1972.

8. G.N. Ramanchandran and A.V. Lakshminarayanan, "Three dimensional reconstructions from radiographs and electron micrographs: Application of convolution instead of Fourier transforms," Proceedings of the National Academy of Sciences, **68**, 2236 - 2240, 1971.

9. G. Herman and A. Naparstek, "Fast image reconstruction based on a Radon inversion formula appropppriate for rapidly collected data," SIAM Journal of Applied Mathematics **33**, 511-533, 1976.

10. J. Radon, "Uber due bestimmung von funktionen durch ihre intergralwerte langsgewisser mannigfaltigkeiten (on the determination of functions from their integrals along certain manifolds," Berichte Saechsische Akademie der Wissenschaften, **29**, pp. 262 - 277, 1917.

11. L. A. Shepp and U. Vardi, “Maximum Likelihood Reconstruction for Emission Tomography” IEEE Trans. Medical Imaging, M1-1, 2 (1982)

12. R. J. Estep, “TGS-Fit: Image Reconstruction Software for Quantitative, Low Resolution Tomographic Assays” Los Alamos National Laboratory” Los Alamos National Laboratory report, LA-12497-MS (1993).

13. R. J. Estep, T. H. Prettyman and G. A. Sheppard, “Tomographic Gamma Scanning to Assay Heterogeneous Radioactive Waste” Nuc. Sci. Eng. **118** 145-152, 183-184 (1993).

14. T. H. Prettyman, R. J. Estep, and G. A. Sheppard, “Development of a tomographic instrument for tomographic nondestructive assay,” Trans. Am. Nuc. Soc. **69** 183-184 (1993). Los Alamos National Laboratory report, LA-UR-93-2580 (1993).

15. R. J. Estep, “A preliminary design Study for Improving Performance in Tomographic Assays” Los Alamos National Laboratory” Los Alamos National Laboratory report, LA-12727-MS (1994).

16. T. H. Prettyman, R. A. Cole, R. J. Estep, and G. A. Sheppard, “A maximum likelihood algorithm for gamma-ray tomographic nondestructive assay,” Nucl. Instr. Meth. **A 356,** 470-475 (1995).

17. 17.. T. H. Prettyman, “Precision estimates for tomographic nondestructive assay,” Proceedings of the 5th International Conference on Facility Operations-Safeguards Interface (American Nuclear Society, Inc., La Grange Park, Illinois 1995), ANS Order No. 700226, pp. 191-199.

18. T. H. Prettyman, L. A. Foster, and R. J. Estep, “Detection and Measurement of Gamma-Ray Self-attenuation in Plutonium Residues.” Proceedings of INMM **37**, 130-136 (1996)

19. T. H. Prettyman, “ARC_TGS User’s Manual,” Los Alamos National Laboratory Transuranic Waste Characterization/Certification Project – Records Management, TWCP-1493 (1998).

20. “Performance Demonstration Program Plan for Nondestructive Assay of Drummed Wastes for the TRU Waste Characterization Program”, Rev 0.1U. S. Dept of Energy, Carlsbad Field Office DOE/CBFO-91-1005 (Mar 22, 2001)

21. T. H. Prettyman, S. E. Betts, D. P. Taggart, R. J. Estep, N. J. Nicholas, M. C. Lucas, and R. A. Harlan, “Field experience with a mobile tomographic nondestructive assay system,” Proceedings of the 4th Nondestructive Assay and Nondestructive Examination Waste Characterization Conference, Salt Lake City, Utah (October 24-26, 1995) 109-137.

22. T. H. Prettyman, S. E. Betts, and A. C. Muscatello and D. Catlett, “Final Report on the Mobile TFS Demonstration at Rocky Flats” Los Alamos National Laboratory report, LA-UR-98-4052 (1998).

23. David J. Mercer, J. Steven Hansen, John P. Lestone, Thomas H. Prettyman, and Larry Kayler, "TGS Measurements of Pyrochemical Salts at Rocky Flats," *proceedings of the Institute of Nuclear Material Management, 42nd Annual Meeting,* Indian Wells, CA, July 15-19, 2001; Los Alamos National Laboratory report LA-UR-01-3509.

24. D. J. Mercer, T. H. Prettyman, M. E. Abhold and S. E. Betts, “Experimental Validation of Tomographic Gamma Scanning for Small Quantities of Special Nuclear Material” Los Alamos National Laboratory report, LA-UR-97-2804 (1997).

25. D. J. Mercer, S. E. Betts, T. H. Prettyman, C. D. Rael, “Tomographic Gamma Scanning of Uranium Contaminated Waste at Rocky Flats” Los Alamos National Laboratory report, LA-UR-98-2922 (1998).

26. . “A Strategic Approach to Integrating the Long-Term Management of Nuclear Materials. The Department of Energy’s Integrated Nuclear Materials Management Plan, A Report to Congress, June, 2000.

27. ”Highly Enriched Uranium, Working Group Report on ES&H Vulnerabilities Associated with the Department’s Storage of Highly Enriched Uranium., US DOE, Dec,1996.

28. J. S. Hansen, unpublished data.

29. J.-P. Francois, “On the Calculation of the Self-Absorption in Spherical Radioactive Sources.” Nucl. Instr. Methods **117**, 153-156 (1974)

30. T.H. Prettyman, J. K. Sprinkle and G. A. Sheppard, “A Weighted Least Squares Lump Correction Algorithm for Transmission Corrected Gamma Ray Non destructive Assay” Nucl. Mat. Manage. **XXII**, 682-690 (1993).

31. T.H. Prettyman, J. K. Sprinkle and G. A. Sheppard, “Performance of an Advanced Lump Correction Algorithm for Gamma Ray Assays of plutonium.” Los Alamos National Laboratory report, LA-UR-94-2477 (1994).

32. T. H. Prettyman, L. A. Foster, and R. J. Estep, "Detection and Measurement of Gamma-Ray Self-Attenuation in Plutonium Residues," Proceedings of INMM (1996) pp. 130-136.